Title
Unexpected variations in the triple oxygen isotope composition of stratospheric carbon dioxide.

Journal
Proceedings of the National Academy of Sciences, 110(44)

Authors
Wiegel, Aaron
Cole, Amanda
Hoag, Katherine
et al.

Publication Date
2013-10-29

DOI
10.1073/pnas.1213082110

Peer reviewed

Unexpected variations in the triple oxygen isotope composition of stratospheric carbon dioxide

Aaron A. Wiegel[a], Amanda S. Cole[a,1], Katherine J. Hoag[b,2], Elliot L. Atlas[c], Sue M. Schauffler[d], and Kristie A. Boering[a,b,3]

Departments of [a]Chemistry and [b]Earth and Planetary Science, University of California, Berkeley, CA 94720; [c]Division of Marine and Atmospheric Chemistry, Rosenstiel School of Marine and Atmospheric Science, University of Miami, Miami, FL 33149; and [d]Earth Observing Laboratory, National Center for Atmospheric Research, Boulder, CO 80307

Edited by Mark H. Thiemens, University of California, San Diego, La Jolla, CA, and approved July 16, 2013 (received for review February 26, 2013)

We report observations of stratospheric CO_2 that reveal surprisingly large anomalous enrichments in ^{17}O that vary systematically with latitude, altitude, and season. The triple isotope slopes reached 1.95 ± 0.05(1σ) in the middle stratosphere and 2.22 ± 0.07 in the Arctic vortex versus 1.71 ± 0.03 from previous observations and a remarkable factor of 4 larger than the mass-dependent value of 0.52. Kinetics modeling of laboratory measurements of photochemical ozone–CO_2 isotope exchange demonstrates that non–mass-dependent isotope effects in ozone formation alone quantitatively account for the ^{17}O anomaly in CO_2 in the laboratory, resolving long-standing discrepancies between models and laboratory measurements. Model sensitivities to hypothetical mass-dependent isotope effects in reactions involving O_3, $O(^1D)$, or CO_2 and to an empirically derived temperature dependence of the anomalous kinetic isotope effects in ozone formation then provide a conceptual framework for understanding the differences in the isotopic composition and the triple isotope slopes between the laboratory and the stratosphere and between different regions of the stratosphere. This understanding in turn provides a firmer foundation for the diverse biogeochemical and paleoclimate applications of ^{17}O anomalies in tropospheric CO_2, O_2, mineral sulfates, and fossil bones and teeth, which all derive from stratospheric CO_2.

For most materials containing oxygen, the relative abundances of its three stable isotopes (^{16}O, ^{17}O, and ^{18}O) fall on a "mass-dependent" fractionation line (1) with a $\ln^{17}O$-$\ln^{18}O$ three-isotope slope[†] near 0.5, which is well-predicted by statistical thermodynamics (3) and chemical reaction rate theories (4). In other words, ^{17}O is usually one-half as depleted or enriched as ^{18}O when measured relative to ^{16}O and relative to those same ratios in an international standard. Discoveries of large deviations from a mass-dependent slope of 0.5 in meteorites (5) and ozone (6, 7), resulting in nonzero ^{17}O anomalies (i.e., $\Delta^{17}O = \ln^{17}O - 0.52\ln^{18}O \neq 0$), have led to many applications tracing the histories and inventories of materials throughout the solar system (1), despite continuing debate about their chemical or physical origins (e.g., refs. 1, 8).

For ozone, the non–mass-dependent enrichments in ^{17}O and ^{18}O have a three-isotope slope of 0.65–1.0 (e.g., ref. 9) and have been traced to anomalous kinetic isotope effects (KIEs) in O_3 formation:

$$O(^3P) + O_2 + M \rightarrow O_3^* + M \rightarrow O_3 + M^*, \qquad [1]$$

where M is any collision partner (10–12). Although much progress has been made in understanding ozone's non–mass-dependent isotopic composition (12–14), the theoretical basis in chemical physics is still unresolved (15–17). In addition, whether ^{17}O anomalies in other species—such as CO_2, N_2O, sulfates, and nitrates (e.g., ref. 18)—result solely from transfer from O_3 or from additional anomalous KIEs remains unclear. Stratospheric CO_2, for example, attains at least part of its observed non–mass-dependent isotopic composition (19–24) via reactions **2**–**3b** (25–28):

$$O_3 + h\nu \rightarrow O(^1D) + O_2(^1\Delta), \qquad [2]$$

$$O(^1D) + CO_2 \rightarrow CO_3^* \rightarrow O(^3P) + CO_2, \qquad [3a]$$

$$O(^1D) + CO_2 \rightarrow CO_3^* \rightarrow O(^1D) + CO_2. \qquad [3b]$$

The observed three-isotope slope for stratospheric CO_2 ranges from ~1.2 to 1.7, much larger than for O_3. To explain the difference, non–mass-dependent isotope effects beyond O_3 formation have been postulated (19, 29), including a coincidental near-resonance for $^{17}O^{12}C^{16}O_2^*$ or a nuclear spin/spin-orbit coupling effect in [**3a**]. In addition, three-isotope slopes for CO_2 measured in laboratory mixtures of UV-irradiated O_2 or O_3 and CO_2 (29–32), slopes calculated from photochemical models of laboratory experiments (30) and the stratosphere (27, 28), and slopes from observations show remarkable disagreements. For example, three-isotope slopes for CO_2 in laboratory experiments typically vary from about 0.8 to 1.0 (29, 30, 32) not the value of 1.7 that has come to be expected for the stratosphere (22, 33). Although one laboratory study has yielded a slope up to 1.8 (31), the experiment was performed at unrealistically high O_3/CO_2 ratios and shows unusual behavior relative to all other published experiments. Experiments under nearly identical conditions but longer irradiation times (32) yielded a slope near 1, suggesting that the higher slope in the high O_3/short irradiation time experiments likely results from non–mass-dependent isotope effects in O_3 photodissociation due to O_3 self-shielding, which is not relevant for atmospheric conditions; thus, the apparent agreement with previous stratospheric observations is arguably fortuitous, as discussed further below. In addition, $\ln^{17}O$ was measured directly in only one previous laboratory study (32), whereas it was inferred from mass balance in all others, which adds additional uncertainty (e.g., if unknown ^{13}C isotope effects might affect the results due to the isobaric interference between $^{13}C^{16}O^{16}O$ and $^{12}C^{17}O^{16}O$ in mass spectrometry measurements). Finally, Liang et al. (27, 28) calculate a three-isotope slope of 1.5 for CO_2 in their model at latitudes >25°N that shows little

Author contributions: E.L.A. and K.A.B. designed research; A.A.W., A.S.C., K.J.H., E.L.A., S.M.S., and K.A.B. performed research; A.A.W., A.S.C., K.J.H., E.L.A., S.M.S., and K.A.B. contributed new reagents/analytic tools; A.A.W., A.S.C., K.J.H., E.L.A., S.M.S., and K.A.B. analyzed data; and A.A.W., A.S.C., K.J.H., E.L.A., and K.A.B. wrote the paper.

The authors declare no conflict of interest.

This article is a PNAS Direct Submission.

[1]Present address: Air Quality Research Division, Environment Canada, Toronto, ON M3H 5T4, Canada.

[2]Present address: US Environmental Protection Agency, San Francisco, CA 94105.

[3]To whom correspondence should be addressed. E-mail: boering@berkeley.edu.

This article contains supporting information online at www.pnas.org/lookup/suppl/doi:10.1073/pnas.1213082110/-/DCSupplemental.

[†]Isotopic compositions are often reported as "δ"-values but a shorthand logarithmic notation is used here, as recommended by Luz and Barkan (2) both for convenience and to avoid unnecessary and uninteresting curvature that the use of δ-values can cause in three-isotope plots for the large laboratory enrichments measured. This logarithmic notation is defined as $\ln^{18}O = \ln[(^{18}O/^{16}O)_{sample}/(^{18}O/^{16}O)_{standard}] = \ln[\delta^{18}O + 1]$, where $(^{18}O/^{16}O)_i$ is the ratio of the number of atoms of ^{18}O to ^{16}O in a sample or standard and $\delta^{18}O = [\{(^{18}O/^{16}O)_{sample}/(^{18}O/^{16}O)_{standard}\}-1]$, and similarly for $\ln^{17}O$ and $\delta^{17}O$.

temporal or spatial variation in the lower and middle stratosphere. The current level of disagreement between experiments, atmospheric observations, and atmospheric modeling shows that isotope exchange between O_3 and CO_2 is still not well understood.

Here, we report measurements of $\ln^{17}O$ and $\ln^{18}O$ of stratospheric CO_2 that reveal much larger three-isotope slopes than expected and their systematic variation with latitude, altitude, and season. We also report time-dependent laboratory and modeling results that demonstrate that anomalous KIEs in O_3 formation alone quantitatively account for the triple isotope composition of CO_2 in the laboratory. Combining laboratory and stratospheric results, we show that differences in temperature, relative rates of mass-dependent reactions, and vertical versus quasihorizontal transport rates can plausibly explain differences in the $\ln^{17}O$-$\ln^{18}O$ relationships between the laboratory and stratosphere and within the stratosphere. The results thus provide a deeper understanding of contemporary stratospheric CO_2 isotope variations, the underlying isotope chemistry, and a sounder foundation for the biogeochemical, paleoclimate, and paleoatmospheric applications of ^{17}O anomalies in materials that derive their signals from stratospheric CO_2 (34–40).

Stratospheric CO_2 was separated cryogenically from whole air samples collected by National Aeronautics and Space Administration (NASA) ER-2 aircraft (41) in winter 1999–2000 during the SAGE III Ozone Loss and Validation Experiment (SOLVE) (42) and a September 2004 balloon flight (43) at 34°N. The isotopic composition was measured on a Finnigan MAT 252 isotope ratio mass spectrometer using the CeO_2 equilibration technique (44). Additional sampling and measurement details are provided in *Materials and Methods* and *SI Appendix*. Results are shown in Fig. 1 and *SI Appendix*, Tables S1–S4. Samples of high-latitude air (>55°N) determined to be in the polar vortex from nitrous oxide (N_2O) and potential temperature (θ) measurements (45) (*SI Appendix*, Fig. S1) exhibit a three-isotope slope from a bivariate linear least-squares regression of 2.22 ± 0.07(1σ). Samples collected at midlatitudes (25–55°N) and in "midlatitude-like" (i.e., nonvortex) air at high latitudes (based on N_2O and θ) yield a three-isotope slope of 1.95 ± 0.05. These slopes are significantly larger (Table 1) than the expected value of 1.71 ± 0.03 from Lämmerzahl et al. (22), with homogeneity of regression tests demonstrating that these differences with respect to the Lämmerzahl data are both significant at the 99% confidence interval (*SI Appendix*, Table S5). If only the new lower stratospheric (<21 km) samples are included in our midlatitude regression, the slope is 1.7 ± 0.2, closer to expectations but more variable. We believe this increased variability in the lower stratosphere is real (see below), although additional uncertainty from a smaller regression range may also contribute.

Additional insight into the regional differences in slope is gained by examining $\Delta\ln^{17}O/\Delta\ln^{18}O$ (i.e., the slope of a line defined by two points: the $\ln^{17}O$ and $\ln^{18}O$ isotopic composition of a sample and the isotopic composition of tropospheric CO_2 with $\ln^{17}O$ = 21.1‰ and $\ln^{18}O$ = 40.2‰) for individual datapoints from the rocket (19) and 2004 balloon datasets. Vertical profiles of CH_4, N_2O, and θ suggest the influence of air transported from more equatorial regions (*SI Appendix*, Figs. S2 and S3 and Table S3). The $\Delta\ln^{17}O/\Delta\ln^{18}O$ values for these tropically influenced samples are typically larger than for samples with more midlatitude-like character based on CH_4, N_2O, and θ. These differences suggest that even larger slopes may be observable in the deep tropics and that transport and mixing of tropical air to 34°N contributes to the $\Delta\ln^{17}O/\Delta\ln^{18}O$ variability in these profiles.

These systematic variations in $\Delta\ln^{17}O/\Delta\ln^{18}O$ and three-isotope slopes with latitude, altitude, and season are not inconsistent with the previous observations of Lämmerzahl et al. (22) at 44°N and 68°N. The narrow range in slope of 1.71 ± 0.03 they measured has been considered the "standard" against which other measurements and model predictions should match (22, 33). However, the

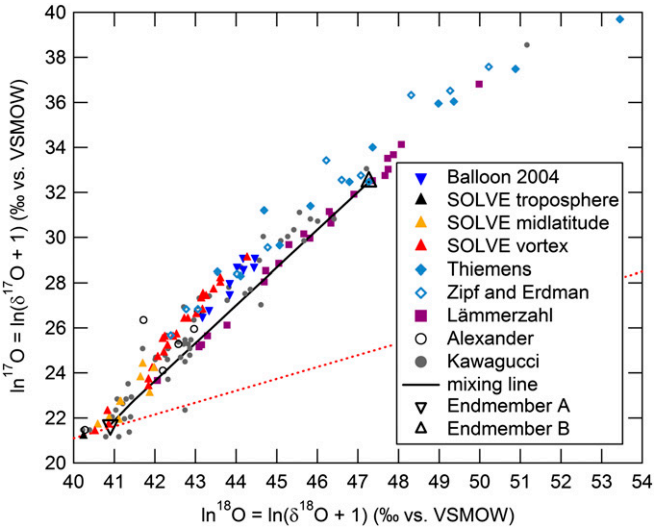

Fig. 1. Stratospheric CO_2 observations. Three isotope plot for the balloon (34°N) and "SOLVE" aircraft (24–83°N) samples, with previous observations: Thiemens (19) and Zipf and Erdman (20) are rocket samples from ~34°N. Lämmerzahl (22) are balloon samples from 44° and 68°N. Alexander (21) are balloon samples from 68°N. Kawagucci (24) are balloon samples from 39° and 68°N. Data from Boering et al. (23) are not shown because of an earlier analytical mass-dependent artifact that affected $\ln^{17}O$ and $\ln^{18}O$ but not $\Delta^{17}O$. The mass-dependent fractionation line with slope 0.528 (red) and a hypothetical end member mixing line (black) with slope 1.7 (*SI Appendix*, Table S6) are also shown. The overall 1σ uncertainties for the SOLVE and Balloon 2004 data including both external precision and accuracy are ±0.1% for $\ln^{18}O$ and ±0.5% for $\ln^{17}O$.

Lämmerzahl flights, based on their timing, would have likely always intercepted nonvortex extratropical air, yielding a relatively homogeneous three-isotope slope not necessarily representative of other regions, similar to how the long-lived tracers CH_4 and N_2O exhibit homogeneous nonvortex extratropical slopes distinct from tropical and vortex slopes. Satellite measurements of CH_4 and N_2O show CH_4:N_2O relationships that are compact (i.e., homogeneous) and distinct between three regions: the tropics, the extratropics, and the polar vortices after significant descent has occurred (46). In contrast, the region at 25 ± 10°N exhibits CH_4:N_2O correlations that are much less compact, consisting of inhomogeneous mixtures of tropical and midlatitude air (46). The CO_2 isotopic composition is also a long-lived tracer (23, 27, 28) because the lifetime for isotope exchange with O_3 is always at least an order of magnitude longer than stratospheric transport timescales, even at 45 km where $O(^1D)$ peaks (27, 28); thus, transport and mixing affect the CO_2 isotopic composition similarly to CH_4 and N_2O. By analogy, homogeneous three-isotope slopes for CO_2 can be observed poleward of 35°N except in Arctic vortex air in January–March (42); the tropical and late vortex three-isotope slopes can be distinct from the nonvortex/extratropical relationships; and the 25 ± 10°N "mixed region" would be an inhomogeneous mixture, as observed. These variations in three-isotope slopes thus appear to be explicable and robust across high-precision CO_2 datasets.

These systematic variations with latitude and season we observe may also account for at least some of the variability in what have been considered to be the noisier datasets shown in Fig. 1 (20, 21, 24). For example, the dataset of Alexander et al. (21) consists of six samples that were collected in or near the polar vortex and which indeed show a higher three-isotope slope of 2.1 ± 0.6(1σ, n = 6), although the variability is high and the uncertainty in slope means it is not statistically different from the previous, lower slope datasets. It is not clear whether the variability is due to the small number of samples and real atmospheric

Table 1. Summary of three isotope slopes for stratospheric CO_2

Source	Dates	Region	Altitude, km	N	Slope, ±1σ
SOLVE	12/99–3/00	High latitude/vortex	11–20	24	2.22 ± 0.07
SOLVE	12/99–3/00	High latitude/nonvortex and midlatitude	11–20	11	1.7 ± 0.2
SOLVE + balloon	12/99–3/00, 9/04	High latitude/nonvortex and midlatitude	11–33	20	1.95 ± 0.05

variability (such as moving in and out of vortex air) or to possible measurement artifacts. Our vortex data and interpretation presented here suggest that at least some of the variability may be real. Similarly, some of Kawagucci et al.'s datapoints (24) overlap with our larger slope datapoints, but they report themselves that a linear fit to their data yields a slope of 1.63 ± 0.05(1σ, n = 58) and that their slope and data in general are not statistically nor characteristically different from the Lämmerzahl et al. dataset. If additional unpublished trace gas data and geophysical parameters are available for their samples, it may be possible to investigate their outliers at larger or smaller $\Delta\ln^{17}O/\Delta\ln^{18}O$ values. Otherwise, whether these outliers are explained by atmospheric variability or by a lower measurement precision for their online CuO equilibration isotope ratio mass spectrometry (IRMS) technique (as the much more scattered relationship between their $\Delta^{17}O$ of CO_2 and N_2O mixing ratio measurements may suggest (*SI Appendix*, Fig. S4) is unclear. Homogeneity of regression tests demonstrate that the differences in slope between our "vortex" and the Kawagucci data and between our "midlatitude" and the Kawagucci data are statistically significant at the 99% and 95% confidence intervals, respectively (*SI Appendix*, Table S5). Finally, the rocket dataset reported by Zipf and Erdman (20), which also lacks information on other long-lived tracer and potential temperature data, overlaps with our dataset, showing a curvilinear $\ln^{17}O$–$\ln^{18}O$ relationship that links our lower and middle stratospheric data with the middle and upper stratospheric rocket data reported by Thiemens et al. (19); this dataset is thus also consistent with the idea that we put forth here that a linear $\ln^{17}O$–$\ln^{18}O$ relationship of 1.7 with a small SD of <0.1 cannot represent the entire stratosphere, in contrast with the now widely held assumption that it does.

To investigate processes that could lead to the larger $\Delta\ln^{17}O/\Delta\ln^{18}O$ values and three-isotope slopes we observe, O_2 and CO_2 mixtures near atmospheric mixing ratios were irradiated with UV light (*Materials and Methods* and *SI Appendix*). The CO_2 isotopic composition was measured (*SI Appendix*, Table S7) and compared with results from a time-dependent photochemical kinetics model we developed using KINTECUS software (*SI Appendix*, Tables S9 and S10). The model accurately predicts both the time dependence and the steady-state values for $\ln^{17}O$, $\ln^{18}O$, and $\Delta^{17}O$ of CO_2 (Fig. 2 and Table 2). These results demonstrate that anomalous KIEs in O_3 formation can quantitatively explain the triple isotope composition of CO_2 in the laboratory at atmospherically relevant O_2, O_3, and CO_2 mixing ratios without invoking additional anomalous KIEs or other unknown effects to account for the data. Importantly, the model uses molecular level rate coefficients without using empirical or phenomenological parameterizations of how the transfer of the anomaly from CO_2 to O_3 occurs at steady state used in previous work (28, 32). These results also demonstrate that slopes close to 1 are to be expected in most laboratory experiments using mercury lamps at atmospherically relevant O_2/CO_2 ratios and pressures below 150 torr. Indeed, even the very high O_3/CO_2 experiments of Shaheen et al. performed for long irradiation times (32) resulted in an experimental slope near 1, as did our photochemical model run under conditions similar to theirs, unlike the slope of 1.8 measured at very high O_3/CO_2 mixing ratios for short irradiation times (31). The short irradiation times combined with the narrow lines of a Hg lamp, large reactor volume, and very high amounts of O_3 in the Chakraborty and Bhattacharya experiments (31) suggest that their 1.8 slope for CO_2 results from non–mass-dependent isotopic self-shielding by O_3 during O_3 photodissociation and subsequent transfer to CO_2 (32) rather than to processes simulating stratospheric isotope photochemistry in their experiment. In other words, isotopic self-shielding by O_3 does not occur at the O_3/CO_2 levels in the atmosphere or in the near-atmospheric mixing ratio laboratory experiments, or even at the longer irradiation times in the high O_3/CO_2 experiments of Shaheen et al.; thus the apparent agreement between the three-isotope slope for CO_2 of 1.8 with the previously expected value of 1.7 is likely fortuitous.

The three-isotope slopes near 1.1 in experiments without isotopic self-shielding artifacts, however, are still much smaller than stratospheric observations. To investigate the possible origins of the laboratory–stratosphere differences in $\Delta\ln^{17}O/\Delta\ln^{18}O$ values, we tested the sensitivity of the photochemical model to various inputs and processes (Fig. 2 and Table 2). Initializing the

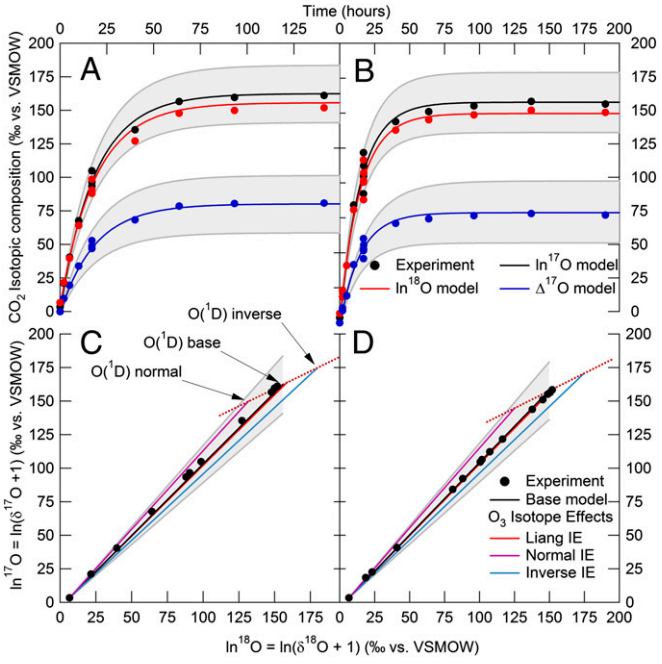

Fig. 2. Experimental versus model results. Time evolution of the CO_2 isotopic composition for the 50 torr (*A*) and 100 torr (*B*) UV irradiation experiments (symbols) and predictions from a photochemical kinetics model (lines). Shaded area shows uncertainty in the base model predictions, dominated by a conservative estimate of the uncertainty in $k_{asymmetric}$ for $^{17}O^{16}O^{16}O$ formation. (*C* and *D*): Same as *A* and *B* in a three-isotope plot. Also included in different model scenarios (*SI Appendix*, Table S10) shown here are theoretical mass-dependent ("MD") isotope effects in O_3 photolysis at 254 nm (48); and large, hypothetical "normal" and "inverse" MD O_3 photolysis isotope effects to illustrate how the three-isotope slope for CO_2 is increased (normal) or decreased (inverse) along a mass-dependent line of slope 0.528 (red dotted line) as the MD isotope effects change the isotopic composition of O_3 and O(^{1}D), while leaving $\Delta^{17}O$ (Table 2) essentially unchanged (to within small differences in the MD coefficients, λ, in $\Delta^{17}O = \ln^{17}O - \lambda\ln^{18}O$, which can range from 0.500 to 0.529; ref. 2). Under these laboratory conditions, there is only one O(^{1}D) isotopic composition, so the CO_2 isotopic composition evolves along a straight line connecting the O(^{1}D) isotopic composition with that of the initial CO_2.

Table 2. Isotopic compositions from photochemistry experiments and kinetics modeling at 50 torr

	CO_2*				O_3†			
Description	$\ln^{17}O$	$\ln^{18}O$	Slope	$\Delta^{17}O$‡	$\ln^{17}O$	$\ln^{18}O$	Slope	$\Delta^{17}O$‡
Experiment	160 ± 1	151 ± 1	1.075 ± 0.004	80.7 ± 1.3	114 ± 7	138 ± 8	0.83 ± 0.07	41 ± 6
Model: base scenario	163	156	1.067	80.3	113	139	0.81	39.2
Liang photolysis IE§	164	159	1.056	80.2	110	134	0.82	39.3
Normal photolysis IE	150	132	1.172	80.4	119	151	0.79	39.2
Inverse photolysis IE	175	180	0.989	79.7	107	127	0.84	39.5
Tropopause O_2 and CO_2	161	153	1.24	80.4	111	136	0.82	39.4
Trop O_2, CO_2, 250 K	140	124	1.41	74.5	96	117	0.83	34.8
Trop O_2, CO_2, 220 K	126	105	1.61	70.7	87	104	0.83	31.8
Trop O_2, CO_2, 200 K	117	92	1.84	68.0	80	95	0.84	29.7

Isotopic compositions are reported in ‰ on the Vienna Standard Mean Ocean Water scale. The modeled $O(^1D)$ isotopic composition is identical to that for CO_2 because isotope effects in the $O(^1D) + CO_2$ isotope exchange reaction were not included in these model scenarios. Results for 100 torr are shown in *SI Appendix*, Table S11.

*Experimental results for CO_2 are an average ($n = 2$, $\pm 1\sigma$) of the measured values at isotopic steady state.

†Experimental results for O_3 are an average ($n = 2$, $\pm 1\sigma$ combined error) of previous results at 50 torr (54, 57).

‡$\Delta^{17}O = \ln^{17}O - 0.528 \ln^{18}O$.

§Theoretical mass-dependent O_3 photolysis isotope effect at 254 nm (48).

model with the tropospheric isotopic compositions of O_2 and CO_2 increases the slope from 1.067 to 1.24, a sensitivity previously noted (28, 31, 32). As the model temperature decreases to stratospheric values, the modeled slope increases further, to 1.84 at 200 K, based on several temperature-dependent O_3 KIE measurements (47) and our estimates of others not yet measured (*SI Appendix*). The temperature decrease changes the predicted magnitudes of the O_3 formation KIEs, which in turn alter the non–mass-dependent isotopic compositions of O_3 and $O(^1D)$ and hence both the three-isotope slope and $\Delta^{17}O$ of CO_2. Introduction of mass-dependent isotope effects in any number of reactions can also change the three-isotope slope but leaves $\Delta^{17}O$ effectively unchanged (Fig. 2 *C* and *D* and Table 2). For example, a mass-dependent O_3 photolysis isotope effect at the experimental wavelength of 254 nm that isotopically depletes the remaining O_3 (48, 49) will mass-dependently enrich $O(^1D)$ and CO_2 and thus decrease the three-isotope slope. Similarly, but with opposite effect, a hypothetical mass-dependent isotope effect that isotopically enriches O_3 will deplete $O(^1D)$ and CO_2, thereby increasing the three-isotope slope. Broadband O_3 photolysis in the stratosphere appears to mass-dependently enrich the remaining O_3 (9), which would increase the slope for CO_2. [Note that the existence of non–mass-dependent isotope effects in ozone photolysis has been proposed (50), but subsequent analysis (51) of those experimental results demonstrated that ozone formation was in fact responsible for the non–mass-dependent enrichments observed.] These experimental and modeling results support the hypothesis (18, 32) that temperature dependence of the O_3 formation KIEs and mass-dependent O_3 photolysis isotope effects likely cause the laboratory–stratosphere differences in the three-isotope slope for CO_2, although differences in the importance of other mass-dependent isotope effects between the laboratory and stratosphere leading to isotopic depletions in $O(^1D)$ or CO_2 cannot be ruled out.

Because the modeled $\ln^{17}O$–$\ln^{18}O$ relationship for CO_2 depends on temperature and O_3 photolysis wavelengths and rates, which vary with altitude and latitude, these variables are the likely origin of the observed regional differences in stratospheric $\ln^{17}O$–$\ln^{18}O$ relationships. Indeed, the O_3 isotopic composition in the upper stratosphere shows regional differences attributed to UV photolysis (9), which was estimated to contribute 25–30% of the total enrichments in tropical O_3 versus only 20–25% at midlatitudes. Our model sensitivities suggest that larger tropical O_3 enrichments would increase the three-isotope slope of tropical CO_2 relative to the extratropics, consistent with inferences from our mixed region observations.

With larger three-isotope slopes in upper tropical CO_2, transport and mixing (which are much faster than CO_2–O_3 isotope exchange) then redistribute this tropical signal to other regions yet keep the slopes distinct, as for the CH_4:N_2O slopes. The larger tropical $\Delta\ln^{17}O/\Delta\ln^{18}O$ values are transported into the mixed region at 25 ± 10°N at 25–40 km and will decrease as mixing into extratropical air proceeds (see below). Similarly, transport of this tropical upper stratospheric air by the residual circulation into the polar vortex generates the high $\Delta\ln^{17}O/\Delta\ln^{18}O$ values there, similar to the winter buildup of O_3 at high latitudes from the tropics (42). Because little photochemistry and vertical mixing occurs in the vortex, and a dynamic barrier at the vortex edge blocks most mixing with midlatitude air, the larger $\Delta\ln^{17}O/\Delta\ln^{18}O$ tropical values are maintained in the vortex. When the vortex breaks up in spring, vortex and midlatitude air mix, decreasing the slope to the extratropical value. For example, apparent vortex remnants sampled in May 1998 at 22 km show a slope of 1.7 (22). Tracer measurements in similar vortex remnants in 1997 demonstrate that such remnants have mixed extensively with midlatitude air by May–June (42, 52). End member mixing of high-N_2O and low-N_2O air produces a mixing line of slope 1.7 (Fig. 1; *SI Appendix*, Table S6) using two samples with ranges of N_2O concentrations similar to air that mixed during and after the 1997 vortex breakup (42, 52) and, more generally, similar to the mixing of low-N_2O and high-N_2O air that occurs on much larger spatial and temporal scales that are known to result in different CH_4:N_2O relationships in the tropics and extratropics (46).

Transport and mixing can also explain the larger scatter in slope in the lower stratosphere noted above. For example, $\Delta\ln^{17}O/\Delta\ln^{18}O$ values for $N_2O < \sim 220$ parts per billion by volume (ppbv) are >1.7, but for $N_2O > \sim 220$ ppbv they vary between ~0.5 and 1.7, are roughly inversely correlated with N_2O, and increase with increasing $\Delta^{17}O$ (Fig. 3). Moreover, the few outliers to the $\Delta^{17}O$ and inverse N_2O trends can be explained by (*i*) the degree of mixing of lower-N_2O air from higher altitudes with higher-N_2O air at lower altitudes, or (*ii*) the fact that the samples are from the lowermost stratosphere ($\theta < 380$ K), which is a mixture of stratospheric air with air recently transported from the troposphere. These characteristics suggest that such lower stratospheric mixing creates real atmospheric variability in $\Delta\ln^{17}O/\Delta\ln^{18}O$ values ranging between the entry (tropospheric) value of ~0.5 to values ≥1.7 (also *SI Appendix*).

In summary, we have shown that room temperature laboratory measurements of CO_2–O_3 isotope exchange near an atmospheric O_2/CO_2 mixing ratio can be quantitatively predicted with a first principles photochemical model and results in a linear

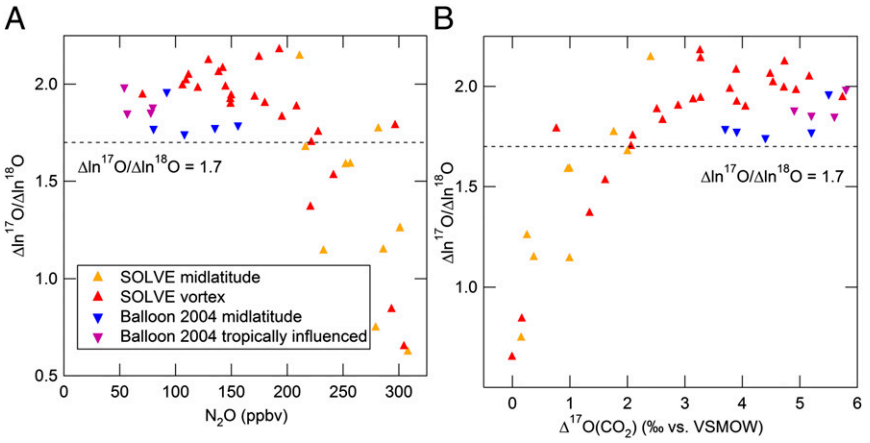

Fig. 3. Variations in $\Delta\ln^{17}O/\Delta\ln^{18}O$ of CO_2. (*A*) $\Delta\ln^{17}O/\Delta\ln^{18}O$ of CO_2 versus N_2O mixing ratio and (*B*) $\Delta\ln^{17}O/\Delta\ln^{18}O$ of CO_2 versus $\Delta^{17}O$ of CO_2; $\Delta\ln^{17}O/\Delta\ln^{18}O$ = 1.7 is shown (dashed line) for reference. In general, the $\Delta\ln^{17}O/\Delta\ln^{18}O$ values increase from a tropospheric, near–mass-dependent value to >1.6 as (*A*) N_2O decreases and (*B*) $\Delta^{17}O$ of CO_2 increases, explaining at least part of the larger observed variability in $\Delta\ln^{17}O/\Delta\ln^{18}O$ in the lower stratosphere where "younger," high N_2O air mixes with "older," lower N_2O air. Note that, for these samples, the trends in $\Delta\ln^{17}O/\Delta\ln^{18}O$ are still apparent (even though the values change) even if we assume that the entry value for $\ln^{18}O$ of CO_2 entering the stratosphere from the troposphere can vary by ±0.5, either by applying the same offset for every point or by mimicking a seasonal variation within the dataset, and even though the overall 1σ uncertainty in the $\ln^{17}O$ measurements including both accuracy and precision is ±0.5%.

$\ln^{17}O$–$\ln^{18}O$ relationship for CO_2 of 1.2 (starting with tropospheric O_2 and CO_2 isotopic compositions), whereas the $\ln^{17}O$–$\ln^{18}O$ relationship for stratospheric CO_2 can vary systematically with latitude, altitude, and time, ranging up to 2.2 in a sometimes curvilinear manner. Model sensitivities suggest that the laboratory–stratosphere and regional stratospheric differences originate from differences in mass-dependent isotope fractionation in O_3 photolysis and in temperature due to the temperature dependence of the non–mass-dependent isotope effects in O_3 formation. The latitude, altitude, and seasonal dependence of the observed three-isotope slopes suggests that stratospheric transport and mixing act to redistribute air with higher $\Delta\ln^{17}O/\Delta\ln^{18}O$ values for CO_2 from the tropical source region to the subtropics and into the polar vortex and then homogenize these higher values to the extratropical background of 1.7. Additional CO_2 isotope measurements in the tropics could validate our hypothesis that the three-isotope slopes are greater there and provide additional constraints on photolysis isotope effects and the temperature dependence of the O_3 formation KIEs, which also need further laboratory investigation. Also, 2D and 3D atmospheric models that include the latitude and altitude dependencies of the isotope chemistry inferred here and that can simulate realistic transport barriers are needed. For ^{17}O anomalies in tropospheric CO_2 (34), in O_2 on short (35, 36) and glacial–interglacial (37, 38) timescales, in ancient mineral sulfates (39), and in fossilized bioapatite (40), we note the following: On one hand, productivity estimates for the current terrestrial and oceanic biospheres are on sounder footing because the isotope chemistry is no longer mysterious. Furthermore, these large three-isotope slopes do not affect previous estimates of the annual mean flux of $\Delta^{17}O$ of CO_2 to the troposphere because $\Delta^{17}O$ is still similarly well-correlated with N_2O in the lower stratosphere (*SI Appendix*, Fig. S4) (23). Importantly, the magnitude of $\Delta^{17}O$ matters more than the magnitude of the three-isotope slopes, a point which is often overlooked. On the other hand, a sensitivity of $\Delta^{17}O$ of CO_2 to the temperature dependence of the anomalous O_3 KIEs represents a possible caveat for longer timescale variations in $\Delta^{17}O$ of O_2, mineral sulfates, and bioapatite. Although Luz et al. (37) already elucidated the need to consider past changes in O_3 and CO_2 levels on $\Delta^{17}O$ of O_2, variations in stratospheric temperatures as climate changes may also affect $\Delta^{17}O$ anomalies, especially if the temperature dependencies of the O_3 KIEs are larger than estimated here.

Materials and Methods

Atmospheric Samples. Air samples were collected between 24°N and 83°N and 11 and 20 km by the Whole Air Sampler instrument during the SOLVE mission (42) in January–March 2000 and at 34.5°N between 27 and 33 km by the Cryogenic Whole Air Sampler instrument aboard a high-altitude scientific balloon (43) launched from Fort Sumner, NM, in September 2004. Mixing ratios of trace gases in the samples were measured at the University of Miami or the National Center for Atmospheric Research, including N_2O and CH_4 using an HP5890 II+ series GC, before shipment to University of California Berkeley (UC Berkeley). At UC Berkeley, CO_2 was separated from air and any residual water in a series of five liquid N_2 and −75.5 °C ethanol–LN_2 traps, respectively. The resulting aliquots of 30–60 μmol of CO_2 were flame sealed into glass ampoules for subsequent IRMS analysis. Several samples exhibited water levels higher than stratospheric air [typically <10 parts per million by volume (ppmv)], indicating the sampler manifolds may have been temporarily contaminated with water. To eliminate potential artifacts from isotope exchange between CO_2 and H_2O either in the sample canisters or during the cryogenic separation that could increase $\Delta\ln^{17}O/\Delta\ln^{18}O$ values, samples with residual water > 20 ppmv have been eliminated from analysis (*SI Appendix*).

Laboratory Experiments. Mixtures of O_2 (Scott Specialty Gases, 99.999%) and CO_2 (Scott Specialty Gases, 99.998%) close to the atmospheric ratio ($O_2/CO_2 \sim 450$) were introduced into a 2.2-L borosilicate glass bulb fitted with a fused quartz (Heraeus-Amersil, Inc.) "finger" extending into the interior of the bulb. A low-pressure Hg/Ar pen lamp (Oriel Instruments) with major emission lines at 184.9 and 253.7 nm was placed in the quartz finger to irradiate the bulb from the center. After irradiation for 0–190 h, the CO_2 and resulting O_3 were separated cryogenically from O_2 using liquid nitrogen and were transferred to a sample tube containing nickel shavings. After heating at 60 °C for 15 min to decompose O_3, the CO_2 was separated cryogenically from the resulting O_2 with liquid nitrogen and then measured by IRMS. In some experiments, the isotopic composition of O_3 was determined by measuring the O_2 from O_3 decomposition at *m/z* values of 32, 33, and 34 by IRMS.

IRMS Measurements. The triple oxygen isotope composition of CO_2 was measured on a Finnigan MAT 252 IRMS at UC Berkeley using the CeO_2 equilibration technique (44) on 12–18-μmol aliquots of the purified CO_2 from the whole air samples or the purified CO_2 from the laboratory experiments. Corrections to the IRMS signals for the presence of N_2O in the stratospheric CO_2 samples before CeO_2 equilibration were made using measurements of the mixing ratio and isotopic composition of N_2O made directly on the stratospheric whole air samples. External 1σ measurement precisions (n = 104 over 2 y) for $\ln^{18}O$, $\ln^{17}O$, and $\Delta^{17}O$ of CO_2 were ±0.05%, ±0.2%, and ±0.2%, respectively, where $\Delta^{17}O = \ln^{17}O - 0.528\ln^{18}O$. Including accuracy (*SI Appendix*) yields overall 1σ uncertainties of ±0.1%, ±0.5%, and ±0.5%, respectively.

Photochemical Kinetics Model. The isotope-specific reaction kinetics occurring in the laboratory reaction bulb was predicted with KINTECUS software (53) using the Modified Bader–Deuflhard integrator to solve the system of stiff differential equations. The model is based on a previous model of O_2–O_3 isotope photochemistry (51) modified to include reactions relevant for CO_2. In the "base model," only KIEs in O_3 formation and $O + O_2$ isotope exchange were included, as measured or derived in earlier studies (10, 11). The pressure dependence of the O_3 formation KIEs was derived from the O_3 formation KIEs at low pressure and the pressure dependence of the O_3 isotopic enrichments (54–56). In the model runs investigating sensitivity to temperature, the temperature dependence of the O_3 formation KIEs was based on a combination of measurements of the temperature dependence of the KIEs for formation of the ^{18}O-containing O_3 isotopomers (47) and the temperature

dependence of the ^{18}O and ^{17}O enrichments in O_3 (9, 47) In model runs investigating sensitivity to possible isotope effects in O_3 photolysis, a theoretical value at 254 nm from Liang et al. (48, 49) was used, as well as hypothetical limiting values for normal and inverse isotope effects. See *SI Appendix* for more details regarding the measurements and calculations.

ACKNOWLEDGMENTS. The stratospheric portion of this work was supported by NASA's Upper Atmosphere Research Program (NNX09AJ95G to the University of California, Berkeley; and NNG05GN80G and NNX09AJ25G to the University of Miami) and the laboratory experiments and kinetics modeling by the National Science Foundation's Experimental Physical Chemistry Program (CHE-0809973 to the University of California, Berkeley).

1. Thiemens MH (2006) History and applications of mass-independent isotope effects. *Annu Rev Earth Planet Sci* 34:217–262.
2. Luz B, Barkan E (2005) The isotopic ratios $^{17}O/^{16}O$ and $^{18}O/^{16}O$ in molecular oxygen and their significance in biogeochemistry. *Geochim Cosmochim Acta* 69(5):1099–1110.
3. Urey HC (1947) The thermodynamic properties of isotopic substances. *J Chem Soc*, 10.1039/JR9470000562.
4. Bigeleisen J, Goeppert Mayer M (1947) Calculation of equilibrium constants for isotopic exchange reactions. *J Chem Phys* 15(5):261–267.
5. Clayton RN, Grossman L, Mayeda TK (1973) A component of primitive nuclear composition in carbonaceous meteorites. *Science* 182(4111):485–488.
6. Thiemens MH, Heidenreich JE, 3rd (1983) The mass-independent fractionation of oxygen: A novel isotope effect and its possible cosmochemical implications. *Science* 219(4588):1073–1075.
7. Mauersberger K (1987) Ozone isotope measurements in the stratosphere. *Geophys Res Lett* 14(1):80–83.
8. Clayton RN (2002) Solar System - Self-shielding in the solar nebula. *Nature* 415(6874): 860–861.
9. Krankowsky D, et al. (2007) Stratospheric ozone isotope fractionations derived from collected samples. *J Geophys Res* 112(D8):D08301.
10. Mauersberger K, Erbacher B, Krankowsky D, Nickel R, Nickel R, Guenther J (1999) Ozone isotope enrichment: Isotopomer-specific rate coefficients. *Science* 283(5400): 370–372.
11. Janssen C, Guenther J, Mauersberger K, Krankowsky D (2001) Kinetic origin of the ozone isotope effect: A critical analysis of enrichments and rate coefficients. *Phys Chem Chem Phys* 3(21):4718–4721.
12. Mauersberger K, Krankowsky D, Janssen C, Schinke R (2005) Assessment of the ozone isotope effect. *Advances in Atomic, Molecular, and Optical Physics*, eds Bederson B, Walther H (Elsevier Academic, San Diego), Vol 50, pp 1–54.
13. Gao YQ, Marcus RA (2001) Strange and unconventional isotope effects in ozone formation. *Science* 293(5528):259–263.
14. Schinke R, Grebenshchikov SY, Ivanov MV, Fleurat-Lessard P (2006) Dynamical studies of the ozone isotope effect: A status report. *Annu Rev Phys Chem* 57:625–661.
15. Ivanov MV, Grebenshchikov SY, Schinke R (2009) Quantum mechanical study of vibrational energy transfer in Ar-O_3 collisions: Influence of symmetry. *J Chem Phys* 130(17):174311.
16. Kryvohuz M, Marcus RA (2010) Coriolis coupling as a source of non-RRKM effects in ozone molecule: Lifetime statistics of vibrationally excited ozone molecules. *J Chem Phys* 132(22):224305.
17. Ghaderi N, Marcus RA (2011) Bimolecular recombination reactions: Low pressure rates in terms of time-dependent survival probabilities, total J phase space sampling of trajectories, and comparison with RRKM theory. *J Phys Chem B* 115(18):5625–5633.
18. Brenninkmeijer CAM, et al. (2003) Isotope effects in the chemistry of atmospheric trace compounds. *Chem Rev* 103(12):5125–5162.
19. Thiemens MH, Jackson T, Zipf EC, Erdman PW, van Egmond C (1995) Carbon dioxide and oxygen isotope anomalies in the mesosphere and stratosphere. *Science* 270: 969–972.
20. Zipf E, Erdman PW (1994) Studies of trace constituents in the upper stratosphere and mesosphere using cryogenic whole air sampling techniques. NASA's Upper Atmosphere Research Program (UARP) and Atmospheric Chemistry Modeling and Analysis Program (ACMAP) Research Summaries 1992–1993: Report to Congress and the Environmental Protection Agency (National Aeronautics and Space Administration, Washington, DC), pp 127-128.
21. Alexander B, Vollmer MK, Jackson T, Weiss RF, Thiemens MH (2001) Stratospheric CO_2 isotopic anomalies and SF_6 and CFC tracer concentrations in the Arctic polar vortex. *Geophys Res Lett* 28(21):4103–4106.
22. Lammerzahl P, Rockmann T, Brenninkmeijer CAM, Krankowsky D, Mauersberger K (2002) Oxygen isotope composition of stratospheric carbon dioxide. *Geophys Res Lett* 29(12):1582.
23. Boering KA, et al. (2004) Observations of the anomalous oxygen isotopic composition of carbon dioxide in the lower stratosphere and the flux of the anomaly to the troposphere. *Geophys Res Lett* 31(3):L03109.
24. Kawagucci S, et al. (2008) Long-term observation of mass-independent oxygen isotope anomaly in stratospheric CO_2. *Atmos Chem Phys* 8:6189–6197.
25. Yung YL, Lee AYT, Irion FW, DeMore WB, Wen J (1997) Carbon dioxide in the atmosphere: Isotopic exchange with ozone and its use as a tracer in the middle atmosphere. *J Geophys Res* 102(D9):10857–10866.
26. Perri MJ, Van Wyngarden AL, Boering KA, Lin JJ, Lee YT (2003) Dynamics of the $O(^1D)$+ CO_2 oxygen isotope exchange reaction. *J Chem Phys* 119(16):8213–8216.
27. Liang MC, Blake GA, Lewis BR, Yung YL (2007) Oxygen isotopic composition of carbon dioxide in the middle atmosphere. *Proc Natl Acad Sci USA* 104(1):21–25.
28. Liang MC, Blake GA, Yung YL (2008) Seasonal cycle of $C^{16}O^{16}O$, $C^{16}O^{17}O$, and $C^{16}O^{18}O$ in the middle atmosphere: Implications for mesospheric dynamics and biogeochemical sources and sinks of CO_2. *J Geophys Res* 113:D12305.
29. Wen J, Thiemens MH (1993) Multi-isotope study of the $O(^1D)$ + CO_2 exchange and stratospheric consequences. *J Geophys Res* 98(D7):12801–12808.
30. Johnston JC, Rockmann T, Brenninkmeijer CAM (2000) $CO_2 + O(^1D)$ isotopic exchange: Laboratory and modeling studies. *J Geophys Res* 105(D12):15213–15229.
31. Chakraborty S, Bhattacharya SK (2003) Experimental investigation of oxygen isotope exchange between CO_2 and $O(^1D)$ and its relevance to the stratosphere. *J Geophys Res* 108(D23):4724.
32. Shaheen R, Janssen C, Rockmann T (2007) Investigations of the photochemical isotope equilibrium between O_2, CO_2 and O_3. *Atmos Chem Phys* 7:495–509.
33. Mauersberger K, Krankowsky D, Janssen C (2003) Oxygen isotope processes and transfer reactions. *Space Sci Rev* 106(1-4):265–279.
34. Hoag KJ, Still CJ, Fung IY, Boering KA (2005) Triple oxygen isotope composition of tropospheric carbon dioxide as a tracer of terrestrial gross carbon fluxes. *Geophys Res Lett* 32(2):L02802.
35. Luz B, Barkan E (2000) Assessment of oceanic productivity with the triple-isotope composition of dissolved oxygen. *Science* 288(5473):2028–2031.
36. Juranek LW, et al. (2012) Biological production in the NE Pacific and its influence on air-sea CO_2 flux: Evidence from dissolved oxygen isotopes and O_2/Ar. *J. Geophys. Res. Oceans* 117:23.
37. Luz B, Barkan E, Bender ML, Thiemens MH, Boering KA (1999) Triple-isotope composition of atmospheric oxygen as a tracer of biosphere productivity. *Nature* 400(6744):547–550.
38. Blunier T, Barnett B, Bender ML, Hendricks MB (2002) Biological oxygen productivity during the last 60,000 years from triple oxygen isotope measurements. *Global Biogeochem Cycles* 16(3):1029.
39. Bao HM, Lyons JR, Zhou CM (2008) Triple oxygen isotope evidence for elevated CO_2 levels after a Neoproterozoic glaciation. *Nature* 453(7194):504–506.
40. Gehler A, Tuetken T, Pack A (2011) Triple oxygen isotope analysis of bioapatite as tracer for diagenetic alteration of bones and teeth. *Palaeogeogr Palaeoclimatol Palaeoecol* 310(1-2):84–91.
41. Flocke F, et al. (1999) An examination of chemistry and transport processes in the tropical lower stratosphere using observations of long-lived and short-lived compounds obtained during STRAT and POLARIS. *J Geophys Res* 104:26625–26642.
42. Newman PA, et al. (2002) An overview of the SOLVE/THESEO 2000 campaign. *J Geophys Res* 107(D20):8259.
43. Froidevaux L, et al. (2006) Early validation analyses of atmospheric profiles from EOS MLS on the Aura satellite. *IEEE Trans Geosci Rem Sens* 44(5):1106–1121.
44. Assonov SS, Brenninkmeijer CAM (2001) A new method to determine the ^{17}O isotopic abundance in CO_2 using oxygen isotope exchange with a solid oxide. *Rapid Commun Mass Spectrom* 15(24):2426–2437.
45. Greenblatt JB, et al. (2002) Tracer-based determination of vortex descent in the 1999/2000 Arctic winter. *J Geophys Res* 107(D20):8279.
46. Michelsen HA, Manney GL, Gunson MR, Zander R (1998) Correlations of stratospheric abundances of CH_4 and N_2O derived from ATMOS measurements. *Geophys Res Lett* 25:2777–2780.
47. Janssen C, Guenther J, Krankowsky D, Mauersberger K (2003) Temperature dependence of ozone rate coefficients and isotopologue fractionation in ^{16}O-^{18}O oxygen mixtures. *Chem Phys Lett* 367(1-2):34–38.
48. Liang MC, Blake GA, Yung YL (2004) A semianalytic model for photo-induced isotopic fractionation in simple molecules. *J Geophys Res* 109(D10):D10308.
49. Liang MC, et al. (2006) Isotopic composition of stratospheric ozone. *J Geophys Res* 111:D02302.
50. Chakraborty S, Bhattacharya SK (2003) Oxygen isotopic fractionation during UV and visible light photodissociation of ozone. *J Chem Phys* 118(5):2164–2172.
51. Cole AS, Boering KA (2006) Mass-dependent and non-mass-dependent isotope effects in ozone photolysis: Resolving theory and experiments. *J Chem Phys* 125(18):184301.
52. Rex M, et al. (1999) Subsidence, mixing, and denitrification of Arctic polar vortex air measured During POLARIS. *J Geophys Res* 104(D21):26611–26623.
53. Ianni JC (2012) KINTECUS, Windows Version 3.962.
54. Morton J, Barnes J, Schueler B, Mauersberger K (1990) Laboratory studies of heavy ozone. *J Geophys Res* 95(D1):901–907.
55. Thiemens MH, Jackson T (1988) New experimental evidence for the mechanism for production of isotopically heavy O_3. *Geophys Res Lett* 15(7):639–642.
56. Thiemens MH, Jackson T (1990) Pressure dependency for heavy isotope enhancement in ozone formation. *Geophys Res Lett* 17(6):717–719.
57. Feilberg KL, Wiegel AA, Boering KA (2013) Probing the unusual isotope effects in ozone formation: Bath gas and pressure dependence of the non-mass-dependent isotope enrichments in ozone. *Chem Phys Lett* 556:1–8.